

# Effects of bulk inversion asymmetry and low interface symmetry on the optical properties of broken-gap heterostructures

I. Semenikhin and A. Zakharova

*Institute of Physics and Technology, Russian Academy of Sciences, Nakhimovskii Avenue 34, Moscow 117218, Russia*

K. Nilsson and K. A. Chao

*Department of Physics, Lund University, Sölvegatan 14A S-22362 Lund, Sweden*

(Received 8 January 2007; revised manuscript received 13 April 2007; published 26 July 2007)

We have studied the influence of bulk inversion asymmetry (BIA) and the relativistic part of the low-symmetry interface Hamiltonian (IH) on intersubband optical transitions, induced by linearly polarized light, between strongly hybridized electron-hole states in asymmetrical InAs/GaSb broken-gap quantum wells grown along the [001] direction. The self-consistent calculations were performed using the Burt-Foreman envelope function theory and a sophisticated eight-band  $\mathbf{k}\cdot\mathbf{p}$  model Hamiltonian. We found that the BIA and the IH can activate originally forbidden spin-flip optical transitions, and that the strength of the corresponding optical matrix elements depends on the light polarization direction and the quasiparticle in-plane wave vector. Both the BIA and the IH contribute significantly to this effect. When the initial electron-hole states are strongly hybridized, the spin-flip optical transition probability can be of the same order as the probability of the spin-conserved transitions. The BIA results in interface-localized terms in the optical matrix elements due to the material-dependent Kane's  $B$  parameter and produces a strong in-plane anisotropy in the absorption of light polarized along the [11] and  $[1\bar{1}]$  directions. The IH also contributes to this effect. We found that the primary contribution to the optical anisotropy comes from the BIA-induced mechanism.

DOI: [10.1103/PhysRevB.76.035335](https://doi.org/10.1103/PhysRevB.76.035335)

PACS number(s): 73.21.Ac, 73.21.Fg, 73.40.Kp

## I. INTRODUCTION

The spin split of the energy levels in semiconductor heterostructures<sup>1–13</sup> introduces a spin dependence not only in the tunneling and magnetotunneling processes<sup>14–22</sup> but also in the intersubband optical transitions induced by linearly polarized light.<sup>6,7,23,24</sup> It is well known that the spin-orbit interaction, structural asymmetry, and bulk inversion asymmetry (BIA) can cause a spin split of the energy levels in nonmagnetic systems in the absence of applied magnetic fields. In zinc-blende heterostructures grown along the [001] direction, the reduced crystal symmetry at the interfaces can cause mixing of the light-hole and heavy-hole states at zero in-plane wave vector,<sup>25,26</sup> as well as a significant in-plane anisotropy in the absorption of linearly polarized light,<sup>27–29</sup> especially for polarizations along the [11] and  $[1\bar{1}]$  directions. These phenomena can be explained within the Burt-Foreman envelope function theory by the linear-in- $\mathbf{k}$  terms in the Hamiltonian, whose effect is largely enhanced in the vicinity of an interface.<sup>30</sup> Similar terms in the low-symmetry interface Hamiltonian (IH) create additional spin splits of the subbands.<sup>6</sup>

There exist only few works on spin-dependent optical transitions induced by linearly polarized light in zinc-blende quantum wells grown along the [001] direction, although there are more studies on transitions induced by circularly polarized light. Due to the spin split of the subbands, the optical transition energy and the corresponding optical matrix elements for an initial state with a given in-plane wave vector are spin dependent.<sup>6,7,23</sup> Under certain conditions, the spin-orbit interaction can stimulate spin-flip optical transitions.<sup>24</sup> As mentioned above, the spin split of the subbands is modified by the BIA and the linear-in- $\mathbf{k}$  IH, which

results in mixing and anticrossing of states with different spins. Hence, the BIA and the linear-in- $\mathbf{k}$  IH are also relevant to the spin-flip processes. The influence of spin mixing on the absorption coefficients and lateral optical anisotropy in GaAs/GaAlAs quantum wells under an external bias was analyzed, taking only the BIA into account.<sup>31</sup> The BIA terms appear in the velocity operator and so in the optical transition operator. The combined effects of the IH and the BIA on the spin-flip transitions and on the in-plane anisotropy of the matrix elements for the [11] and the  $[1\bar{1}]$  light polarization directions are so far not studied.

The situation becomes more complicated in broken-gap heterostructures where the hybridization of electron, light-hole, and heavy-hole states changes the spin split of the subbands. Hence, the effects of the BIA and the IH on the spin-dependent optical transitions are further modified. We thus expect an emergence of interesting features which we will examine in the present work.

The active region of a typical broken-gap heterostructure is an InAs/GaSb quantum well sandwiched between two wide-gap AlSb barriers. The InAs conduction band overlaps with the GaSb valence band. If at zero in-plane wave vector,  $\mathbf{k}_{\parallel}=0$ , the lowest electron level in the InAs layer lies below the highest hole level in the GaSb layer, these levels may anticross at some finite  $\mathbf{k}_{\parallel}$ . The hybridization gap formed in the in-plane dispersion was observed experimentally<sup>32,33</sup> and analyzed theoretically.<sup>6–9</sup> For quasiparticle states with  $\mathbf{k}_{\parallel}$  along the [10] direction, the hybridization effects on the optical matrix elements were studied<sup>7</sup> for light polarizations along and perpendicular to the sample growth direction. In this study (Ref. 7), the BIA and the IH were neglected, and therefore two of the four possible transitions between the states of the two pairs of spin-split subbands were found to

be forbidden. For transitions from the zone-center states in InAs/GaSb superlattices, it was found<sup>6,28</sup> that the in-plane anisotropy of the optical matrix elements is very small when the BIA-induced terms are ignored in the optical transition operator.

The eight-band  $\mathbf{k}\cdot\mathbf{p}$  model Hamiltonian used in our present study on optical transitions in broken-gap heterostructures includes not only the BIA and the IH but also the lattice-mismatch induced strain. Based on the complicated eight-band Hamiltonian, self-consistent calculations were recently performed to examine the quasiparticle cyclotron masses and effective  $g$  factors in InAs/GaSb quantum wells.<sup>34</sup> It was found that self-consistency is essential for deriving accurate results.

We will use the Burt-Foreman envelope function theory to calculate self-consistently the subband dispersions and the associated optical matrix elements in AlSb/InAs/GaSb/AlSb quantum wells grown along the [001] direction. For a thorough understanding of the strain effect, we will consider quantum wells grown on both InAs and on GaSb substrates, since different substrates generate different amount of lattice-mismatch induced strain in the quantum well.

In Sec. II, we will describe our model Hamiltonian and show the subband dispersion which we will need to define the optical transitions. The optical matrix elements will be analyzed and calculated in Sec. III, where the symmetry effect will be demonstrated. The optical anisotropy with respect to different light polarizations will be studied in Sec. IV. A conclusion will follow in Sec. V. The BIA and the IH terms in the Hamiltonian are listed in Appendix A, and the explicit form of velocity operator is given in Appendix B.

## II. MODEL HAMILTONIAN AND ENERGY DISPERSION

We consider an AlSb/InAs/GaSb/AlSb quantum well connected at both ends to either InAs or GaSb contact layers, and analyze this system with an eight-band  $\mathbf{k}\cdot\mathbf{p}$  Hamiltonian at the  $\Gamma$  point using the Burt-Foreman envelope function theory. The  $z$  axis is along the growth direction [001], and the  $x$  and  $y$  axes are along the [100] and [010] directions, respectively. With the set of basis functions<sup>9</sup>

$$S\uparrow, X\uparrow, Y\uparrow, Z\uparrow, S\downarrow, X\downarrow, Y\downarrow, Z\downarrow, \quad (1)$$

the Hamiltonian can be expressed as

$$\hat{H} = \begin{pmatrix} \hat{H}_4 & 0 \\ 0 & \hat{H}_4 \end{pmatrix} + \hat{H}_{SO} + \hat{H}_\epsilon + \hat{H}_{ek} + \hat{H}_B + \hat{H}_k. \quad (2)$$

The  $4 \times 4$  matrix  $\hat{H}_4$  depends on the conduction band edge  $E_C$ , the valence band edge  $E_V$ , the momentum operators, the interband momentum matrix elements  $P(z)$ , and the modified Luttinger parameters. The spin-orbit interaction is described by the term  $\hat{H}_{SO}$ . The matrix  $\hat{H}_\epsilon$  is the lattice-mismatch induced strain independent of the momentum operators. The explicit expressions of  $\hat{H}_4$ ,  $\hat{H}_{SO}$ , and  $\hat{H}_\epsilon$  can be found in Ref. 9 and will not be repeated here. The BIA Hamiltonian  $\hat{H}_{ek}$

+  $\hat{H}_B$  and the IH  $\hat{H}_k$  are not considered in existing works on optical transitions in broken-gap heterostructures, and their explicit expressions are given in Appendix A. The operators in  $\hat{H}_{ek}$  are proportional to the strain tensor components  $\epsilon_{ij}$  and the momentum operator components  $\hat{k}_j$ , and  $\hat{H}_B$  depends on Kane's  $B$  parameter. Equations (A6)–(A8) in Appendix A give the matrix representation of the IH  $\hat{H}_k$ , which consists of two parts. The part containing the factor  $[C_{40}, \hat{k}_z]$  is the relativistic term, and the part containing the factor  $\Omega_j \delta(z-z_j)$  is the nonrelativistic term, where  $z_j$  is the position of the  $j$ th interface.  $C_{40}$  is a material parameter, and  $\Omega_j$  depends on the materials at both sides of the interface. For the AlSb/InAs/GaSb/AlSb quantum well to be studied here, there is so far no published value of  $\Omega_j$ , and the nonrelativistic term will be ignored in our numerical calculation. This simplification will not change our final conclusion qualitatively, and will be discussed in detail later. We should point out that since both  $[C_{40}, \hat{k}_z]$  and  $\Omega_j \delta(z-z_j)$  are finite only at the interfaces, they are proportional to each other near the  $j$ th interface. Consequently, the IH  $\hat{H}_k$  is linear in  $\mathbf{k}$ .

The subband dispersions and the corresponding wave functions are derived from the Schrödinger equation

$$\hat{H}\Psi = E\Psi, \quad (3)$$

where  $\Psi$  is the multicomponent envelope function and  $E$  the corresponding energy. We use the basis-expansion method given in Ref. 34 to solve the Schrödinger equation self-consistently together with the Poisson equation. The subband anisotropy in the quantum well is ignored in the charge-density calculations. The numerical error created by this simplification is negligibly small as discussed in Ref. 35. We will here not repeat the details of the numerical computation which is well documented in Refs. 34 and 35.

There are two commonly studied broken-gap heterostructures with the same quantum well AlSb/InAs/GaSb/AlSb as the active region. The GaSb-based type is the GaSb/AlSb/InAs/GaSb/AlSb/GaSb structure grown on GaSb with two  $p$ -doped GaSb contacts, and the InAs-based type is the InAs/AlSb/InAs/GaSb/AlSb/InAs structure grown on InAs with two  $n$ -doped InAs contacts. Since the term  $\hat{H}_{ek}$  changes the dispersions in the valence band, its effects are stronger in the InAs-based structures where the GaSb layer in the quantum well is strained. We will present our numerical results calculated for the GaSb-based structures, since if the influence of BIA and IH is important in GaSb-based structures, it may be even more influential in the InAs-based structures.

For the numerical calculations, we set the thicknesses of the AlSb, InAs, and GaSb layers in the active region to 10 nm. The acceptor concentration in the GaSb contacts is  $10^{18} \text{ cm}^{-3}$ . The deformation potentials, stiffness constants, and lattice constants are available in Ref. 36, and the energy gaps, split-off energies, interband momentum matrix elements, conduction and valence band offsets, and the Luttinger parameters are found in Ref. 7. The material parameters  $C_4$ ,  $B$ , and  $C_{40}$ , which are introduced in Appendix A and listed in Table I, are taken from Refs. 5, 11, and 30,

TABLE I. Numerical values of the material parameters used in the BIA terms and the IH.  $B$  is taken from Ref. 11,  $C_4$  from Ref. 5, and  $C_{40}$  from Ref. 30.

	InAs	GaSb	AlSb
$B$ (eV Å <sup>2</sup> )	13.7	49.9	0
$C_4$ (eV Å)	2.9	2.2	3.7
$C_{40}$ (eV Å)	-0.01	-0.23	-0.23

respectively. Our self-consistent calculations are performed at the low temperature of 4.2 K. The so-obtained energy-band-edge diagram is shown in Fig. 1, where the solid lines are for the conduction band edge and the dashed lines are for the valence band edge.

The calculated dispersions for in-plane wave vector  $\mathbf{k}_{\parallel}$  along the [10] and [11] directions in the two-dimensional Brillouin zone are shown in Fig. 2 with the Fermi level indicated by the dashed line. According to the characteristic features of the wave functions at  $\mathbf{k}_{\parallel}=0$ , the six subbands of interest are labeled as  $1hh$ ,  $2hh$ , and  $3hh$  for the heavy-hole-like subbands, as  $1e$  and  $2e$  for the electronlike subbands, and as  $1lh$  for the light-hole-like subband. With increasing magnitude of  $\mathbf{k}_{\parallel}$ , the characters of subband can change. For example, the  $1e$  and the  $1hh$  subbands anticross and interchange their character around  $k_{\parallel}=0.1$  nm<sup>-1</sup>, where a hybridization gap between the two subbands is formed.

For finite  $\mathbf{k}_{\parallel}$ , each subband splits due to the Rashba effect, the BIA, and the low  $C_{2v}$  symmetry of the IH. We found that among the three terms  $\hat{H}_{ek}$ ,  $\hat{H}_B$ , and  $\hat{H}_k$ , only the spin split contributed by the BIA mechanism is significant for all subbands at large  $k_{\parallel}$ . The spin-split anisotropy exhibited in Fig. 2 is mainly due to the BIA and the structural asymmetry. Similar features in broken-gap heterostructures were investigated previously.<sup>10-12</sup> It is interesting to point out that the states of the  $1hh$  (or any other) subband with different spins anticross

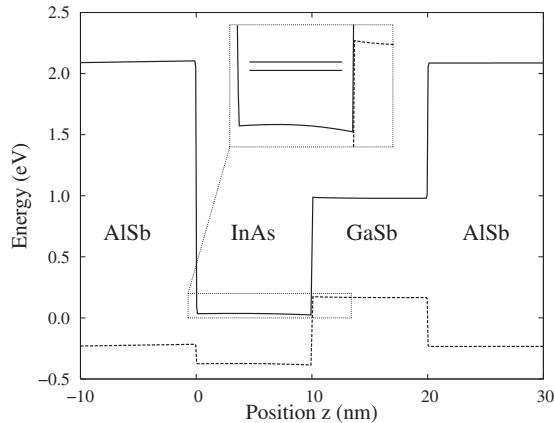


FIG. 1. The self-consistent energy-band-edge diagram of a GaSb-based AlSb/InAs/GaSb/AlSb quantum well grown along the [001] direction. The solid lines are for the conduction band edge and the dashed lines are for the valence band edge. The inset shows the magnification of the region where the InAs conduction band overlaps with the GaSb valence band as well as the positions of the lowest electronlike level  $1e$  and highest heavy-hole level  $1hh$ .

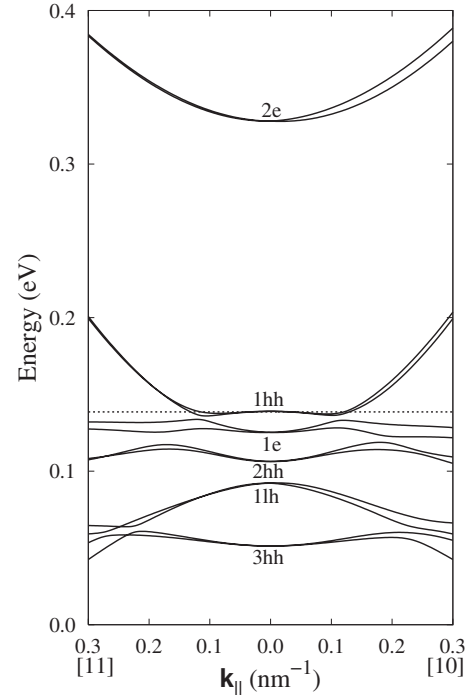


FIG. 2. The subband dispersions in the GaSb-based InAs/GaSb quantum well along the [10] direction (right half) and along the [11] direction (left half). The zero energy is set at the InAs conduction band edge at the AlSb/InAs interface. The Fermi-level position is marked with the dashed horizontal line.

because of their mixing due to the BIA and IH unless the in-plane wave vector  $\mathbf{k}_{\parallel}$  is along the [11] direction. If  $\mathbf{k}_{\parallel}$  is along the [11] direction, the levels cross. If the BIA and IH are neglected, the  $1hh$  levels cross also for  $\mathbf{k}_{\parallel}$  along the [10] direction. In the low-symmetry directions, on the other hand, the warping terms in Hamiltonian mix states with different spins, which results in an anticrossing behavior. This anticrossing or crossing appears in the vicinity of the hybridization gap between the  $1e$  and  $1hh$  subbands. The  $1hh$  and  $1e$  levels with different spins may also anticross for all directions of  $\mathbf{k}_{\parallel}$  except for the [11] direction. Comparing our self-consistent subband dispersions with those obtained in Ref. 9, we see that the charge redistribution changes the ordering of levels and shifts the positions of hybridization gaps to lower  $k_{\parallel}$ . This certainly influences the optical matrix elements, which will be examined in the next section.

### III. OPTICAL MATRIX ELEMENTS

To calculate the optical transition probability between the state  $l$  in one subband and the state  $k$  in another subband, we first define the velocity operator

$$\hat{v} = \frac{1}{\hbar} \frac{\partial \hat{H}}{\partial \hat{\mathbf{k}}} = \hat{v}_0 + \hat{v}_1. \quad (4)$$

In the above expression,

$$\hbar\hat{\mathbf{v}}_0 = \begin{pmatrix} \partial\hat{H}_4/\partial\hat{\mathbf{k}} & 0 \\ 0 & \partial\hat{H}_4/\partial\hat{\mathbf{k}} \end{pmatrix} \quad (5)$$

is the contribution from  $\hat{H}_4$ , and

$$\hbar\hat{\mathbf{v}}_1 = \frac{\partial\hat{H}_B}{\partial\hat{\mathbf{k}}} + \frac{\partial\hat{H}_{ek}}{\partial\hat{\mathbf{k}}} \quad (6)$$

is the contribution from the symmetry-related terms  $\hat{H}_{ek}$  and  $\hat{H}_B$ . The operators  $\hat{\mathbf{v}}_0$  and  $\hat{\mathbf{v}}_1$  are given in Appendix B. The IH  $\hat{H}_k$  does not contribute to the velocity operator because the various terms cancel. Hence,  $\hat{H}_k$  affects the optical absorption only through its effect on the wave functions of the hybridized electron-hole states. Through the boundary conditions,  $\hat{H}_k$  introduces an additional light-hole–heavy-hole mixing which exists even at zero in-plane wave vector.

With  $\mathbf{e}$  as the light polarization unit vector, the optical transition operator is defined<sup>37</sup> as  $\mathbf{e} \cdot \hat{\mathbf{v}}$ . The optical matrix element is

$$M = (2m)^{1/2} \langle \Psi_k | \mathbf{e} \cdot \hat{\mathbf{v}} | \Psi_l \rangle, \quad (7)$$

where  $m$  is the free electron mass. If in the operator  $\hat{H}$  in Eq. (4) we keep only terms proportional to the interband momentum matrix element  $P(z)$ , then Eq. (7) reduces to the commonly used equation for the optical matrix element,

$$M = \left( \frac{2}{m} \right)^{1/2} \langle \psi_k | \mathbf{e} \cdot \hat{\mathbf{p}} | \psi_l \rangle, \quad (8)$$

where  $\psi_k$  and  $\psi_l$  are Bloch functions, and  $\hat{\mathbf{p}}$  is the momentum operator. We should point out that in Eq. (8), the effect of remote bands is neglected in the optical transition operator. Consequently, the effect of BIA is ignored.

In a complete Hamiltonian, instead of the eight-band model Hamiltonian considered here, all bands are taken into account. In this case, across each interface, every state in each band contributes to the optical matrix elements in a continuous fashion. In our eight-band  $\mathbf{k} \cdot \mathbf{p}$  model Hamiltonian, the remote bands are treated with perturbation theory and thus their contributions to the optical matrix elements are localized at the interfaces. Although a similar interface contribution also comes from the  $\hat{H}_4$  term in Eq. (2), the relevant physical process is clearly embedded in the operator  $\hat{H}_B$  which contains elements of the form  $\hat{k}_z B \hat{k}_l$ . If the light polarization is along the  $l$  axis, there is a term proportional to  $\hat{k}_z B(z)$  in the transition operator. Since  $B(z)$  is discontinuous at each interface, the operator  $\hat{k}_z B(z)$  will generate terms proportional to  $\delta(z - z_j)$ , where  $z_j$  marks the position of the  $j$ th interface. This is the physical origin of the specific interface contribution to the optical matrix elements.

For different light polarization directions, we will calculate  $|M_0|^2 \equiv |\hbar M / \sqrt{2m}|^2$  along various in-plane wave vector directions and use the numerical results to demonstrate the symmetry effects of the BIA and IH. The position of the Fermi energy in Fig. 2 suggests that the important optical processes are the  $1hh$ - $2e$  transition between the states in the

$1hh$  and  $2e$  subbands and the  $1e$ - $2e$  transition between the states in the  $1e$  and  $2e$  subbands. A non-self-consistent calculation, using a simpler Hamiltonian without the BIA terms ( $\hat{H}_{ek}$  and  $\hat{H}_B$ ) and the IH term ( $\hat{H}_k$ ), was performed in Ref. 7 to study these two  $1hh$ - $2e$  and  $1e$ - $2e$  transitions. At  $\mathbf{k}_\parallel \neq 0$ , each level in Fig. 2 splits into two, and thus there are four possible optical transitions; two are named spin-conserved transitions and two are named spin-flip transition. All four transitions were found in Ref. 7 if the in-plane wave vector  $\mathbf{k}_\parallel$  is along a low-symmetry direction, such as [12]. However, for  $\mathbf{k}_\parallel$  along a high-symmetry direction such as [10] or [11], only the two spin-conserved transitions were allowed for light polarization along the growth direction,  $\mathbf{e} \parallel \mathbf{z}$ . It is then interesting to demonstrate whether the BIA and IH terms can activate the two forbidden spin-flip transitions. In the following, we will present our numerical results for  $\mathbf{k}_\parallel$  along the [10] ([01]) axis and the [11] axis, but not along any low-symmetry direction. In order to compare our results with Ref. 7, we will use the notation introduced in Ref. 7 to label the two spin-split dispersion branches of each energy level. In Fig. 2, in the region of small  $k_\parallel$ , the lower dispersion branch is assigned with a subscript  $a$  and the upper with a subscript  $b$ . It is important to notice that with increasing  $k_\parallel$ , the two spin-split branches may cross. When this happens, the  $a$  branch lies above the  $b$  branch. We should keep this in mind when we come to interpret our numerical results.

For the convenience of description, we define  $\hat{H}_0$  as the simplified version of the full Hamiltonian  $\hat{H}$  excluding the BIA and IH terms  $\hat{H}_{ek}$ ,  $\hat{H}_B$ , and  $\hat{H}_k$ . Let us first analyze the behavior of  $|M_0|^2$  for  $\mathbf{e} \parallel \mathbf{z}$ . For the  $1hh$ - $2e$  transition with  $\mathbf{k}_\parallel$  along the [10] direction, the results are shown in Fig. 3, where panel (a) is calculated with  $\hat{H}_0$  and panel (b) with  $\hat{H}$ . The two curves in Fig. 3(a) are due to the spin-conserved  $1hh_b$ - $2e_a$  transition (solid curve) and  $1hh_a$ - $2e_b$  transition (dashed curve). When the BIA and the IH terms are included, the originally forbidden spin-flip transitions are activated. Hence, in Fig. 3(b) there are four curves representing the  $1hh_b$ - $2e_a$  transition (solid curve), the  $1hh_a$ - $2e_b$  transition (dashed curve), the  $1hh_a$ - $2e_a$  transition (dotted curve), and the  $1hh_b$ - $2e_b$  transition (dash-dotted curve). The spin-conserved transitions are represented by the dotted and dash-dotted curves for large  $k_\parallel$ . For small  $k_\parallel$ , the spin-up and spin-down states of the  $1hh$  subband are mixed. Comparing panels (a) and (b) and checking with Fig. 2, it is clear that the two spin-flip transitions are activated in the region of  $k_\parallel$  where the  $1hh$  level and the  $1e$  level anticross and strongly hybridize. Then, the values of  $|M_0|^2$  for the spin-flip transitions are of the order of those for the spin-conserved transitions. In the region of large  $k_\parallel$ , the  $1hh$ - $2e$  transition is actually of the character of the transition between the first and second electronlike subbands. The heavy-hole-like states are mainly localized in the GaSb layer and the electronlike states in the InAs layer, and consequently  $|M_0|^2$  of the  $1hh$ - $2e$  transition is large only for large  $k_\parallel$ . Also, we have found that the optical matrix elements are zero at  $k_\parallel = 0$  in Fig. 3(a), while they are negligibly small but nonzero in Fig. 3(b) due to the light- and heavy-hole mixing caused by  $\hat{H}_k$ .

Similar plots but for the  $1e$ - $2e$  transition are shown in Fig. 4, where the solid, dashed, dotted, and dash-dotted curves

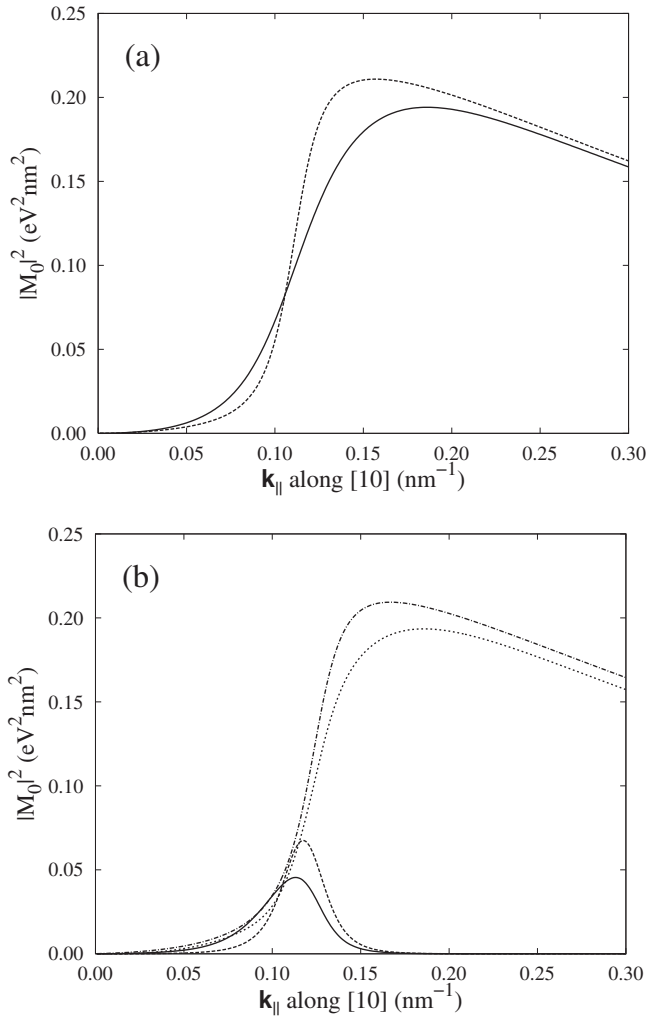


FIG. 3. Square of the absolute value of the optical matrix element for transitions between the states in the  $1hh$  and  $2e$  subbands. Light polarization is along the  $z$  axis and  $\mathbf{k}_{\parallel}$  is along the  $[10]$  direction. Panel (a) is calculated with  $\hat{H}_0$  and panel (b) with  $\hat{H}$ . The solid, dashed, dotted, and dash-dotted curves represent, respectively, the  $1hh_b-2e_a$ ,  $1hh_a-2e_b$ ,  $1hh_a-2e_a$ , and  $1hh_b-2e_b$  transitions.

represent, respectively, the  $1e_b-2e_a$ ,  $1e_a-2e_b$ ,  $1e_a-2e_a$ , and  $1e_b-2e_b$  transitions. Again, we see that the spin-flip transitions are activated by the BIA and IH terms in the region of  $k_{\parallel}$  where the  $1hh$  subband and the  $1e$  subband are close. Here for large  $k_{\parallel}$ , the  $1e-2e$  transition is essentially of the  $1hh-2e$  character, resulting in a vanishing  $|M_0|^2$ . We should mention that spin-conserved transitions similar to those in Figs. 3(a) and 4(a) were obtained in Ref. 7.

To separate the effects of the IH and the BIA terms, we have calculated the optical matrix elements for the  $1e-2e$  transitions with  $\hat{H}_k$  neglected but with BIA included. The result is shown in Fig. 5, where we note that at  $k_{\parallel}=0$  the sum of the two  $|M_0|^2$  values for the spin-conserved and spin-flip transitions is almost equal to that in Fig. 4(b), and exactly equal to the  $|M_0|^2$  in Fig. 4(a) where only the spin-conserved transitions are present. Comparing these three figures, it is clear that both the BIA term and the IH term shift the optical transitions from the spin-conserved channel to the spin-flip

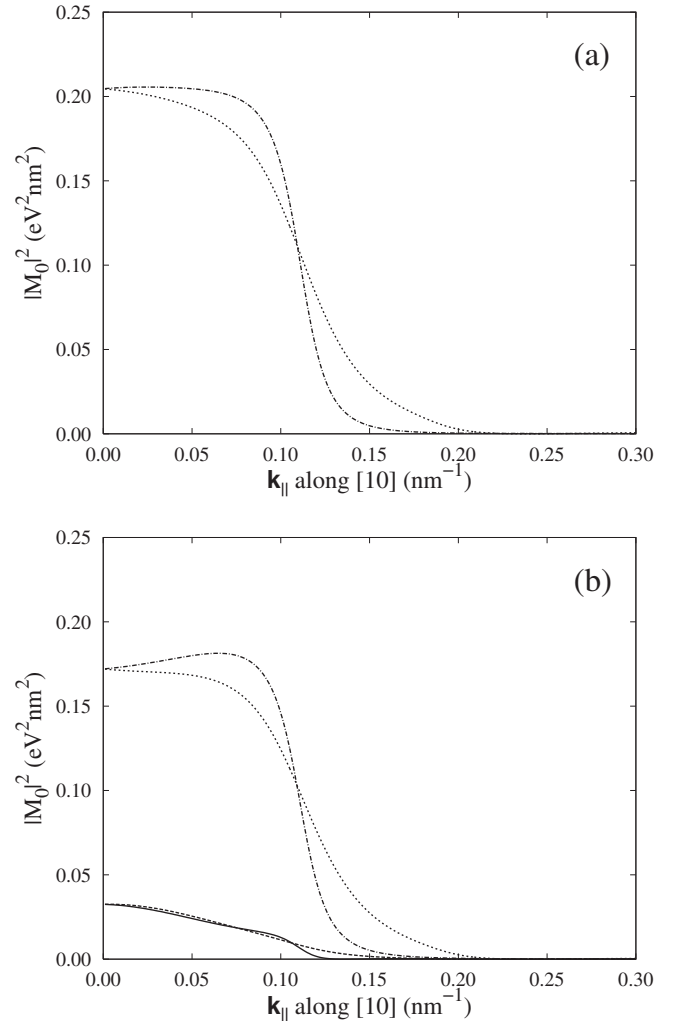


FIG. 4. Same as in Fig. 3 but for transitions between the states in the  $1e$  and  $2e$  subbands. The solid, dashed, dotted, and dash-dotted curves represent, respectively, the  $1e_b-2e_a$ ,  $1e_a-2e_b$ ,  $1e_a-2e_a$ , and  $1e_b-2e_b$  transitions.

channel. While the effect of the BIA term appears in both spin-state mixing and in the velocity operator, the IH term does not contribute to the velocity operator at all. The IH term  $\hat{H}_k$  affects the optical transitions solely by changing the wave functions.

The situation becomes quite different if we change the direction of  $\mathbf{k}_{\parallel}$  from  $[10]$  to  $[11]$ . For  $\mathbf{e} \parallel \mathbf{z}$  again, the calculated  $|M_0|^2$  is shown in Fig. 6 with the solid, dashed, dotted, and dash-dotted curves representing, respectively, the  $1hh_b-2e_a$ ,  $1hh_a-2e_b$ ,  $1e_a-2e_a$ , and  $1e_b-2e_b$  transitions. These results, derived with the full Hamiltonian  $\hat{H}$  including both the BIA and the IH terms, do not show any activated spin-flip transitions. We would again like to point out that at  $k_{\parallel}=0$  the value of  $|M_0|^2$  for the  $1e-2e$  transition in Fig. 6 is exactly the same as the sum of the two  $|M_0|^2$  for the spin-conserved and spin-flip transitions in Fig. 4(b), but nearly the same as that in Fig. 4(a), as it should be. When  $|M_0|^2$  is calculated with  $\hat{H}_0$  only, the result is almost identical to that obtained with full Hamiltonian, in agreement with Ref. 7.

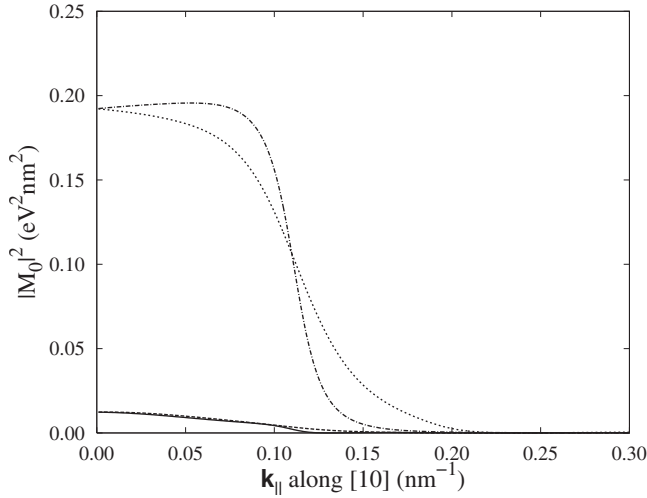


FIG. 5. Square of the absolute value of the optical matrix element for the  $1e-2e$  transitions obtained without the IH term. Light polarization is along the  $z$  axis and  $\mathbf{k}_{\parallel}$  is along the  $[10]$  direction. The transition labels are the same as in Fig. 4.

Hence, for  $\mathbf{k}_{\parallel}$  along the  $[11]$  direction, the effect of the BIA and IH terms on the optical transition is mainly quantitative but not qualitative, because the BIA and IH do not mix states with different spins.

Since the optical matrix elements depend on the directions of both  $\mathbf{k}_{\parallel}$  and  $\mathbf{e}$ , we change the light polarization direction from the  $z$  axis to the  $x$  axis and to the  $y$  axis to further investigate the effect of BIA and IH. For the  $1hh-2e$  transitions with  $\mathbf{k}_{\parallel}$  along the  $[10]$  direction, the calculated  $|M_0|^2$  using the full Hamiltonian is plotted in Fig. 7(a) for  $\mathbf{e}\parallel\mathbf{x}$  and in Fig. 7(b) for  $\mathbf{e}\parallel\mathbf{y}$ . All four spin-conserved and spin-flip transitions are obtained. However, similar calculations, with the BIA and IH terms excluded, yield only two spin-conserved transitions for  $\mathbf{e}\parallel\mathbf{x}$  and two spin-flip transitions for

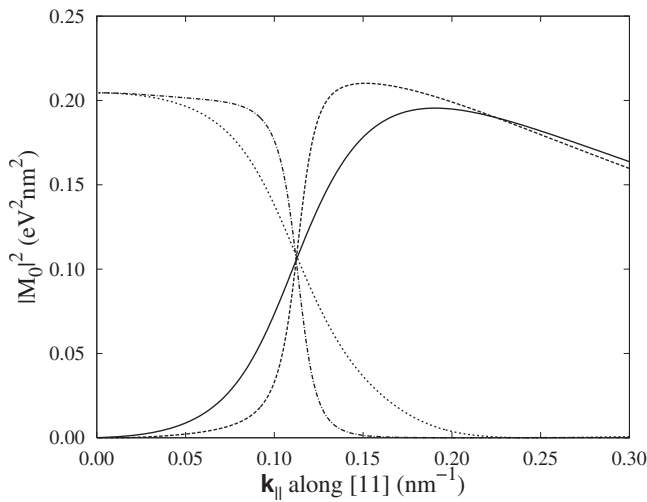


FIG. 6. Square of the absolute value of the optical matrix element for  $\mathbf{k}_{\parallel}$  along the  $[11]$  direction with light polarization along the  $z$  axis. The solid, dashed, dotted, and dash-dotted curves represent, respectively, the  $1hh_b-2e_a$ ,  $1hh_a-2e_b$ ,  $1e_a-2e_a$ , and  $1e_b-2e_b$  transitions.

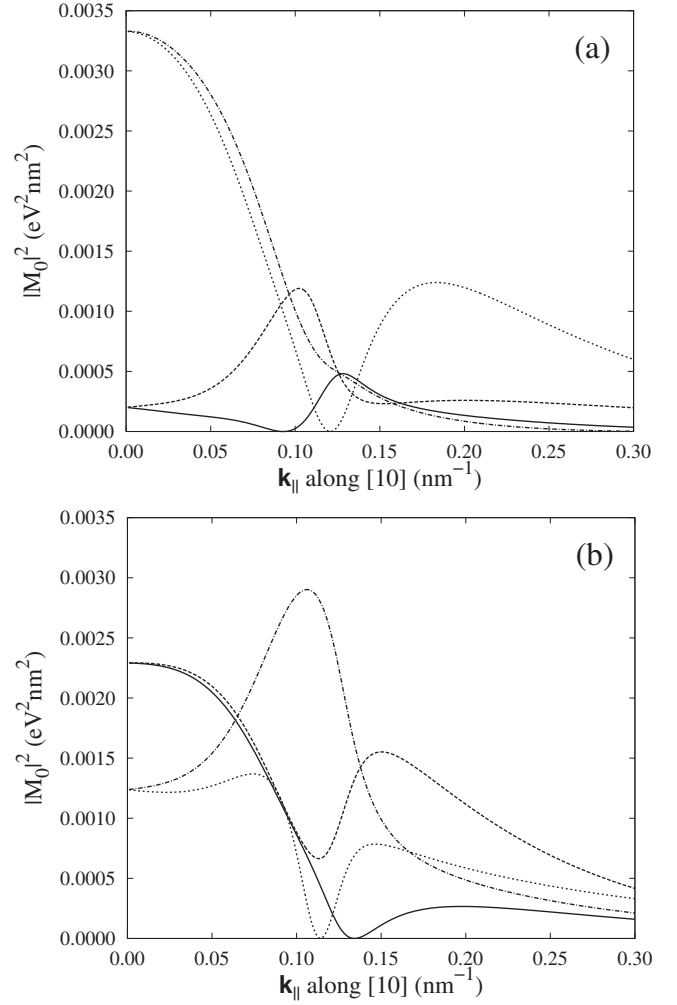


FIG. 7. Square of the absolute value of the optical matrix element for the transitions between the states in the  $1hh$  and  $2e$  subbands, calculated with the full Hamiltonian for  $\mathbf{k}_{\parallel}$  along the  $[10]$  direction. Panel (a) is for light polarization along the  $x$  axis, and panel (b) along the  $y$  axis. The solid, dashed, dotted, and dash-dotted curves represent, respectively, the  $1hh_b-2e_a$ ,  $1hh_a-2e_b$ ,  $1hh_a-2e_a$ , and  $1hh_b-2e_b$  transitions.

$\mathbf{e}\parallel\mathbf{y}$ . It is worthwhile to notice that for  $\mathbf{e}\parallel\mathbf{x}$  and  $\mathbf{e}\parallel\mathbf{y}$ , the value of  $|M_0|^2$  is 2 orders of magnitude smaller than for  $\mathbf{e}\parallel\mathbf{z}$ .

We have analyzed in detail the cases where  $\mathbf{k}_{\parallel}$  is along the high-symmetry directions  $[10]$  and  $[11]$ . Lowering the symmetry by including the BIA and the IH terms activates the spin-flip transitions. When  $\mathbf{k}_{\parallel}$  deviates from the high-symmetry axes,  $|M_0|^2$  remains finite for the spin-flip transitions even when the BIA and the IH terms are neglected. This is due to the contribution from the warping terms in the Hamiltonian.

#### IV. OPTICAL ANISOTROPY

The numerical results presented above suggest a strong anisotropy of the optical matrix elements with respect to the light polarization. It was shown<sup>29</sup> that the low  $C_{2v}$  symmetry of the IH causes such anisotropy with respect to in-plane

light polarization in type-II superlattices. Similar phenomenon was obtained for the far-infrared transitions in InAs/GaSb superlattices.<sup>6,28</sup> The reason is the nonequivalence of the [11] and the  $[1\bar{1}]$  directions caused by the interface symmetry. This type of nonequivalence can also be achieved in asymmetrical quantum wells due to the BIA.<sup>12</sup> Here, we will investigate the combined effect of the BIA and IH terms on the optical anisotropy. For a given light polarization  $\mathbf{e}$  and a given in-plane wave vector  $\mathbf{k}_{\parallel}$ , and for optical transitions between subbands  $\alpha$  and  $\beta$ , we first define a quantity

$$I_{\alpha\beta}(\mathbf{e}, \mathbf{k}_{\parallel}) = \sum_{i,j} |M_{ij}(\mathbf{e}, \mathbf{k}_{\parallel})|^2, \quad (9)$$

where  $i$  runs over the states in the  $\alpha$  subband and  $j$  runs over the states in the  $\beta$  subband. Then, the optical anisotropy with respect to the light polarizations  $\mathbf{e}_1$  and  $\mathbf{e}_2$  can be measured by the polarization

$$\lambda_{\alpha\beta} = \frac{I_{\alpha\beta}(\mathbf{e}_2, \mathbf{k}_{\parallel}) - I_{\alpha\beta}(\mathbf{e}_1, \mathbf{k}_{\parallel})}{I_{\alpha\beta}(\mathbf{e}_2, \mathbf{k}_{\parallel}) + I_{\alpha\beta}(\mathbf{e}_1, \mathbf{k}_{\parallel})}. \quad (10)$$

If  $\mathbf{e}_1$  is along the [10] direction and  $\mathbf{e}_2$  along the [01] direction, at  $\mathbf{k}_{\parallel}=0$ ,  $\lambda_{\alpha\beta}=0$  and there is no optical anisotropy.

For our numerical calculation, we set  $\mathbf{e}_1$  along the [11] direction and  $\mathbf{e}_2$  along the  $[1\bar{1}]$  direction. We again consider the high-symmetry situation where  $\mathbf{k}_{\parallel}$  is along the [10] direction. In this case, if we remove the BIA and the IH terms from the full Hamiltonian  $\hat{H}$ , we find  $\lambda_{\alpha\beta}=0$ . To separate the effect of BIA and the effect of IH, we will therefore calculate  $\lambda_{\alpha\beta}$  twice: first with the full Hamiltonian  $\hat{H}$  and then with the partial Hamiltonian  $\hat{H}-\hat{H}_k$ . The so-obtained polarization  $\lambda_{\alpha\beta}$  is shown in Fig. 8(a). The  $1hh-2e$  and  $1e-2e$  transitions, calculated with the full Hamiltonian, are marked with the solid and the dashed curves, respectively. For both transitions, the degree of polarization is substantial for the entire range of  $k_{\parallel}$ . When the IH term  $\hat{H}_k$  is removed from  $\hat{H}$ , the polarization is reduced from the solid curve to the dotted curve for the  $1hh-2e$  transition, and from the dashed curve to the dash-dotted curve for the  $1e-2e$  transition. Apparently, the primary contribution to the polarization is from the BIA term, and the IH term is only a secondary effect. Since the BIA does not contribute to the wave functions at  $\mathbf{k}_{\parallel}=0$ , the polarization in this case is mainly due to the contribution from BIA to the velocity operator. We also show in Fig. 8(b) the  $\lambda_{\alpha\beta}$  calculated for  $\mathbf{k}_{\parallel}$  along the [11] direction. In Ref. 6, where InAs/GaSb superlattices were considered, the large in-plane anisotropy was obtained for the far-infrared transitions between the  $1e$  and  $1hh$  subbands in the vicinity of the hybridization gap. Our calculations also show an increased anisotropy for the  $1hh-2e$  optical transitions when the initial  $1hh$  states anticross with the  $1e$  states. We have again found a very small contribution of the IH to the lateral optical anisotropy.

The effect on lateral optical anisotropy suggested by our numerical results can be detected by measuring the variation of the absorption coefficients when the light polarization direction is changed within the  $xy$  plane. Such experiments

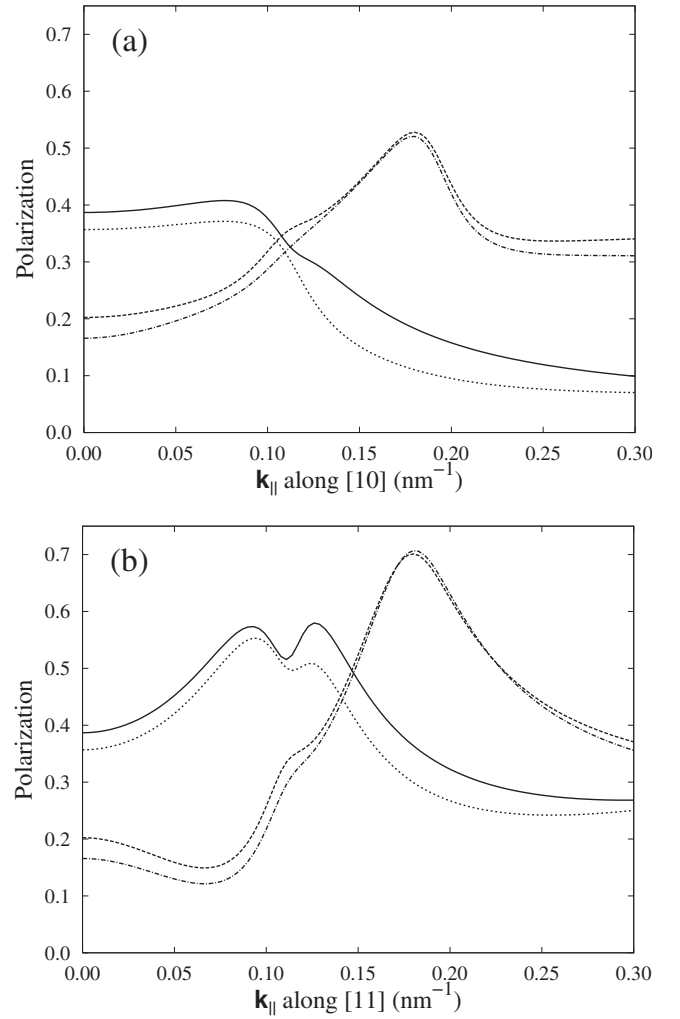


FIG. 8. Optical anisotropy for  $\mathbf{k}_{\parallel}$  (a) along the [10] direction and (b) along the [11] direction. Solid and dashed curves are for the  $1hh-2e$  and  $1e-2e$  transitions, respectively. The corresponding dependences obtained neglecting the term  $\hat{H}_k$  are shown in dotted and dash-dotted curves.

were already performed in InAs/AlSb superlattices.<sup>38</sup> If we decrease the thickness of the InAs and/or the GaSb layer, the percentage contribution from the interface region to the optical matrix elements is increased, and so an enhanced lateral optical anisotropy is expected. We have confirmed this conjecture with numerical calculations.

## V. CONCLUSION

With accurate self-consistent calculations, we have demonstrated that the bulk inversion asymmetry and the low  $C_{2v}$  symmetry of the interfaces can activate originally forbidden optical transitions, induced by linearly polarized light, between subbands in broken-gap heterostructures containing an InAs/GaSb quantum well. The originally forbidden spin-flip transitions can be activated for light polarizations along the growth direction or along the direction of  $\mathbf{k}_{\parallel}$ . On the other hand, when the light is polarized in the plane perpendicular

to  $\mathbf{k}_{\parallel}$ , the originally forbidden spin-conserved transitions can be activated. The value of the optical matrix element of the activated spin-flip transition depends on the light polarization direction  $\mathbf{e}$  and the carrier in-plane wave vector  $\mathbf{k}_{\parallel}$ , and can be of the same order as that of the spin-conserved transitions. The in-plane optical anisotropy is significant for the  $[11]$  and  $[\bar{1}\bar{1}]$  light polarization directions with the main contribution from the bulk inversion asymmetry induced terms in the transition operator for  $\mathbf{k}_{\parallel} \approx 0$ .

Among the two types of commonly studied broken-gap heterostructures, the GaSb-based and the InAs-based, we have presented our numerical results for GaSb-based heterostructures. However, we have performed similar calculations for InAs-based heterostructures, and only found quantitative differences between the results of these two structure types. In InAs-based structures, the strained GaSb layer in the well quantitatively modifies the light-hole–heavy-hole mixing for small  $k_{\parallel}$ , and hence the mixing of the light-hole and the heavy-hole states with the electron states. One example of this quantitative change appears in the optical anisotropy; for small  $k_{\parallel}$ , the contribution from the IH term  $\hat{H}_k$  to the optical polarization for the  $1e$ - $2e$  transitions is much larger in InAs-based heterostructures than in GaSb-based ones. Furthermore, the activation of spin-flip optical transitions by the term  $\hat{H}_{ek}$  is stronger in InAs-based structures.

As mentioned earlier, the matrix representation of the IH  $\hat{H}_k$  consists of two parts, as given by Eqs. (A6)–(A8) in Appendix A. The part containing the factor  $[C_{40}, \hat{k}_z]$  is the relativistic term, and the part containing the factor  $\Omega_j \delta(z - z_j)$  is the nonrelativistic term.<sup>30,39</sup> The nonrelativistic term was studied for a GaAs/AlAs(001) heterointerface and produces a small shift of energy levels about 1 meV.<sup>30</sup> The parameter  $\Omega$  depends on the GaAs/AlAs(001) interface condition.<sup>39</sup> Its value is about 0.19 eV Å for a smooth waffle interface, about 0.30 eV Å for an abrupt waffle interface, about 0.082 eV Å for an abrupt planar interface, and about 0.056 eV Å for a smooth planar interface. At the same GaAs/AlAs(100) interface, the relativistic contribution is measured by the difference  $\Delta C_{\text{GaAs/AlAs}}$  between the  $C_{40}$  value for GaAs and the  $C_{40}$  value for AlAs, which is<sup>30</sup>  $\Delta C_{\text{GaAs/AlAs}} = 0.02$  eV Å. Therefore, for the GaAs/AlAs(100) interface, the dominating contribution to light-hole–heavy-hole mixing comes from the nonrelativistic term in the IH  $\hat{H}_k$ .

For the InAs/GaSb(100) interface, there are very few similar calculations of  $C_{40}$  and  $\Omega$ . While  $\Delta C_{\text{InAs/GaSb}} = 0.22$  eV Å can be found in the literature,<sup>30</sup> to our knowledge the value of  $\Omega$  is not available. Consequently, in the present work we cannot calculate the nonrelativistic contribution to the light-hole–heavy-hole mixing. Nevertheless, the BIA and the low-symmetry IH have a strong influence on the optical properties of broken-gap heterostructures even when the nonrelativistic term is ignored, as we have demonstrated here. It is not unreasonable to expect a stronger influence if the nonrelativistic term is included. Our findings in this paper are correct at least at the semiquantitative level with possible improvements on the numerical accuracy.

## ACKNOWLEDGMENT

This work was financially supported by the RFBR.

## APPENDIX A

In this appendix, we give explicit expressions of the operators  $\hat{H}_{ek}$ ,  $\hat{H}_B$ , and  $\hat{H}_k$ .

$$\hat{H}_{ek} = C_4(\epsilon_{zz} - \epsilon_{xx}) \begin{pmatrix} \hat{H}_{0k} & \hat{H}_+ \\ \hat{H}_- & \hat{H}_{0k} \end{pmatrix}, \quad (\text{A1})$$

where  $C_4$  is a material constant, and  $\epsilon_{zz}$  and  $\epsilon_{xx}$  are strain tensor components ( $\epsilon_{xx} = \epsilon_{yy}$ ). The matrices  $H_{0k}$  and  $H_{\pm}$  are

$$\hat{H}_{0k} = \frac{1}{2} \begin{pmatrix} 0 & 0 & 0 & 0 \\ 0 & 0 & 0 & i\hat{k}_y \\ 0 & 0 & 0 & i\hat{k}_x \\ 0 & -i\hat{k}_y & -i\hat{k}_x & 0 \end{pmatrix} \quad (\text{A2})$$

and

$$\hat{H}_{\pm} = \begin{pmatrix} 0 & 0 & 0 & 0 \\ 0 & -(\hat{k}_x \pm i\hat{k}_y) & 0 & 0 \\ 0 & 0 & -(\hat{k}_x \pm i\hat{k}_y) & 0 \\ 0 & 0 & 0 & -(\hat{k}_x \pm i\hat{k}_y) \end{pmatrix}. \quad (\text{A3})$$

The matrix  $\hat{H}_B$  has the form

$$\hat{H}_B = \begin{pmatrix} \hat{H}_{B0} & 0 \\ 0 & \hat{H}_{B0} \end{pmatrix}, \quad (\text{A4})$$

where the matrix  $\hat{H}_{B0}$  contains operators of the type  $\hat{k}_j B \hat{k}_l$ . We use the symmetrized form of each element in  $\hat{H}_{B0}$  because, to our knowledge, its exact form is still unknown. The nonzero terms in  $\hat{H}_{B0}$  are

$$\begin{aligned} \hat{H}_{B0_{21}} = \hat{H}_{B0_{12}} &= \frac{1}{2}(\hat{k}_y B \hat{k}_z + \hat{k}_z B \hat{k}_y), \\ \hat{H}_{B0_{31}} = \hat{H}_{B0_{13}} &= \frac{1}{2}(\hat{k}_x B \hat{k}_z + \hat{k}_z B \hat{k}_x), \\ \hat{H}_{B0_{41}} = \hat{H}_{B0_{14}} &= \frac{1}{2}(\hat{k}_y B \hat{k}_x + \hat{k}_x B \hat{k}_y). \end{aligned} \quad (\text{A5})$$

The above matrices are defined using the basis functions in Eq. (1). They were obtained by applying a unitary transformation to the corresponding matrices in Ref. 40.

To present the matrix  $\hat{H}_k$ , we start with the matrix in Ref. 30 which includes the relativistic part of IH for the basis set in which the Hamiltonian is diagonal at  $\mathbf{k}=0$ . We will neglect the linear-in- $\mathbf{k}$  bulk inversion asymmetry terms which are strain independent because they are small. Hence, the



constants  $C_3$  and  $C_5$  in this Hamiltonian are set to zero. Also, we only take the terms corresponding to the  $\Gamma_8$  band into account because the split-off band states lie much below the hybridized electron-hole states which we consider here. After applying a unitary transformation to reach the basis set in Eq. (1) and adding the nonrelativistic part of IH from Ref. 39, we have

$$\hat{H}_k = \begin{pmatrix} \hat{H}_{k0} & \hat{H}_{k+} \\ \hat{H}_{k-} & \hat{H}_{k0} \end{pmatrix}, \quad (\text{A6})$$

where

$$\hat{H}_{k0} = \left\{ -\frac{i}{3}[C_{40}, \hat{k}_z] + \sum_j \Omega_j \delta(z - z_j) \right\} \begin{pmatrix} 0 & 0 & 0 & 0 \\ 0 & 0 & 1 & 0 \\ 0 & 1 & 0 & 0 \\ 0 & 0 & 0 & 0 \end{pmatrix} \quad (\text{A7})$$

and

$$\hat{v}_x = \begin{pmatrix} 0 & iP & \frac{1}{2}(B\hat{k}_z + \hat{k}_z B) & Bk_y \\ -iP & 2Lk_x & Nk_y & N_+ \hat{k}_z + \hat{k}_z N_- \\ \frac{1}{2}(B\hat{k}_z + \hat{k}_z B) & Nk_y & 2Mk_x & 0 \\ Bk_y & N_- \hat{k}_z + \hat{k}_z N_+ & 0 & 2Mk_x \end{pmatrix}, \quad (\text{B2})$$

$$\hat{v}_y = \begin{pmatrix} 0 & \frac{1}{2}(B\hat{k}_z + \hat{k}_z B) & iP & Bk_x \\ \frac{1}{2}(B\hat{k}_z + \hat{k}_z B) & 2Mk_y & Nk_x & 0 \\ -iP & Nk_x & 2Lk_y & N_+ \hat{k}_z + \hat{k}_z N_- \\ Bk_x & 0 & N_- \hat{k}_z + \hat{k}_z N_+ & 2Mk_y \end{pmatrix}, \quad (\text{B3})$$

$$\hat{v}_z = \begin{pmatrix} 0 & Bk_y & Bk_x & iP \\ Bk_y & M\hat{k}_z + \hat{k}_z M & 0 & Nk_x \\ Bk_x & 0 & M\hat{k}_z + \hat{k}_z M & Nk_y \\ -iP & Nk_x & Nk_y & L\hat{k}_z + \hat{k}_z L \end{pmatrix}. \quad (\text{B4})$$

In Eqs. (B2)–(B4), the terms proportional to Kane's  $B$  parameter define the operator  $\hat{v}_B$ , and the remaining terms define the operator  $\hat{v}_0$ . The material parameters  $M$ ,  $L$ ,  $N$ ,  $N_+$ , and  $N_-$  are functions of the coordinate  $z$ , and can be ex-

$$\hat{H}_{k\pm} = -\frac{1}{3}[C_{40}, \hat{k}_z] \begin{pmatrix} 0 & 0 & 0 & 0 \\ 0 & 0 & 0 & 1 \\ 0 & 0 & 0 & \pm i \\ 0 & -1 & \mp i & 0 \end{pmatrix}. \quad (\text{A8})$$

The constant  $C_{40}$  is renamed from the constant  $C_4$  defined by Eq. (4) in Ref. 30. The constant  $\Omega_j$  is the coupling constant for the light-hole–heavy-hole mixing at the  $j$ th interface located at  $z=z_j$ . The terms proportional to  $C_{40}$  are of relativistic origin,<sup>30</sup> while the terms proportional to  $\Omega_j$  are the nonrelativistic contribution.<sup>39</sup> In a heterostructure  $B$ ,  $C_4$ , and  $C_{40}$  are all material dependent.

## APPENDIX B

In this appendix, we will give the explicit form of the velocity operator. Let us define the contribution to the velocity operator from the term  $\hat{H}_B$  as  $\hat{v}_B$  and from the term  $\hat{H}_{ek}$  as  $\hat{v}_e$ . Then, we have  $\hat{v}_1 = \hat{v}_B + \hat{v}_e$ . The block diagonal  $\hat{H}_B$  is already defined in Appendix A with two identical blocks  $\hat{H}_{B0}$ . Since  $\hat{v}_0$  is also block diagonal, we have

$$\hbar(\hat{v}_0 + \hat{v}_B) = \sum_{j=x,y,z} \mathbf{n}_j \begin{pmatrix} \hat{v}_j & 0 \\ 0 & \hat{v}_j \end{pmatrix}, \quad (\text{B1})$$

where  $\mathbf{n}_x$ ,  $\mathbf{n}_y$ , and  $\mathbf{n}_z$  are unit vectors, and

pressed in terms of the modified Luttinger parameters.<sup>9</sup>

The operator  $\hat{H}_{ek}$  contributes only to the  $x$  and  $y$  components of the velocity operator. Let us define

$$GX = \frac{1}{C_4(\epsilon_{zz} - \epsilon_{xx})} \hbar v_{ex} \quad (\text{B5})$$

and

$$GY = \frac{1}{C_4(\epsilon_{zz} - \epsilon_{xx})} \hbar v_{ey}, \quad (\text{B6})$$

where  $v_{ex}$  and  $v_{ey}$  are the components of  $\hat{v}_e$ . Then, the non-zero components of  $GX$  are  $GX_{34}=GX_{78}=i/2$ ,  $GX_{43}=GX_{87}$

$=-i/2$ , and  $GX_{26}=GX_{37}=GX_{48}=GX_{62}=GX_{73}=GX_{84}=-1$ . The nonzero components of  $GY$  are  $GY_{24}=GY_{68}=i/2$ ,  $GY_{42}=GY_{86}=-i/2$ ,  $GY_{26}=GY_{37}=GY_{48}=-i$ , and  $GY_{62}=GY_{73}=GX_{84}=i$ .

- 
- <sup>1</sup>E. I. Rashba, *Sov. Phys. Solid State* **2**, 1109 (1960); Yu. A. Bychkov and E. I. Rashba, *JETP Lett.* **39**, 78 (1984).  
<sup>2</sup>F. T. Vasko and N. A. Prima, *Sov. Phys. Solid State* **21**, 994 (1979).  
<sup>3</sup>J. Luo, H. Munekata, F. F. Fang, and P. J. Stiles, *Phys. Rev. B* **38**, 10142 (1988); **41**, 7685 (1990).  
<sup>4</sup>V. M. Edelstein, *Solid State Commun.* **73**, 233 (1990).  
<sup>5</sup>M. Silver, W. Batty, A. Ghiti, and E. P. O'Reilly, *Phys. Rev. B* **46**, 6781 (1992).  
<sup>6</sup>R. Magri, L. W. Wang, A. Zunger, I. Vurgaftman, and J. R. Meyer, *Phys. Rev. B* **61**, 10235 (2000).  
<sup>7</sup>E. Halvorsen, Y. Galperin, and K. A. Chao, *Phys. Rev. B* **61**, 16743 (2000).  
<sup>8</sup>A. Zakharova, S. T. Yen, and K. A. Chao, *Phys. Rev. B* **64**, 235332 (2001).  
<sup>9</sup>A. Zakharova, S. T. Yen, and K. A. Chao, *Phys. Rev. B* **66**, 085312 (2002).  
<sup>10</sup>X. Cartoixa, D. Z.-Y. Ting, and T. C. McGill, *Phys. Rev. B* **68**, 235319 (2003).  
<sup>11</sup>X. Cartoixa, D. Z.-Y. Ting, and T. C. McGill, e-print arXiv:cond-mat/0212394.  
<sup>12</sup>I. Vurgaftman and J. R. Meyer, *Phys. Rev. B* **70**, 115320 (2004).  
<sup>13</sup>A. Zakharova, I. Lapushkin, K. Nilsson, S. T. Yen, and K. A. Chao, *Phys. Rev. B* **73**, 125337 (2006).  
<sup>14</sup>Calvin Yi-Ping Chao and S. L. Chuang, *Phys. Rev. B* **43**, 7027 (1991).  
<sup>15</sup>A. Zakharova, F. T. Vasko, and V. Ryzhii, *J. Phys.: Condens. Matter* **6**, 7537 (1994).  
<sup>16</sup>A. Voskoboinikov, S. S. Liu, and C. P. Lee, *Phys. Rev. B* **58**, 15397 (1998).  
<sup>17</sup>A. Voskoboinikov, S. S. Liu, C. P. Lee, and O. Tretyak, *J. Appl. Phys.* **87**, 387 (2000).  
<sup>18</sup>David Z.-Y. Ting and X. Cartoixa, *Phys. Rev. B* **68**, 235320 (2003).  
<sup>19</sup>A. E. Botha and M. R. Singh, *Phys. Rev. B* **67**, 195334 (2003).  
<sup>20</sup>V. I. Perel', S. A. Tarasenko, I. N. Yassievich, S. D. Ganichev, V. V. Bel'kov, and W. Prettl, *Phys. Rev. B* **67**, 201304(R) (2003).  
<sup>21</sup>I. Vurgaftman and J. R. Meyer, *Phys. Rev. B* **67**, 125209 (2003).  
<sup>22</sup>A. Zakharova, K. Nilsson, K. A. Chao, and S. T. Yen, *Phys. Rev. B* **72**, 115329 (2005).  
<sup>23</sup>Yia-Chung Chang and J. N. Schulman, *Phys. Rev. B* **31**, 2069 (1985).  
<sup>24</sup>R. J. Warburton, C. Gauer, A. Wixforth, J. P. Kotthaus, B. Brar, and H. Kroemer, *Phys. Rev. B* **53**, 7903 (1996).  
<sup>25</sup>M. S. Kiledjian, J. N. Schulman, K. L. Wang, and K. V. Rousseau, *Surf. Sci.* **267**, 405 (1992).  
<sup>26</sup>E. L. Ivchenko, A. Yu. Kaminski, and U. Rössler, *Phys. Rev. B* **54**, 5852 (1996).  
<sup>27</sup>O. Krebs and P. Voisin, *Phys. Rev. B* **61**, 7265 (2000).  
<sup>28</sup>L. W. Wang, S. H. Wei, T. Mattila, A. Zunger, I. Vurgaftman, and J. R. Meyer, *Phys. Rev. B* **60**, 5590 (1999).  
<sup>29</sup>E. L. Ivchenko and M. O. Nestoklon, *Phys. Rev. B* **70**, 235332 (2004).  
<sup>30</sup>Bradley A. Foreman, *Phys. Rev. Lett.* **86**, 2641 (2001).  
<sup>31</sup>Bang-fan Zhu and Yia-Chung Chang, *Phys. Rev. B* **50**, 11932 (1994).  
<sup>32</sup>M. J. Yang, C. H. Yang, B. R. Bennett, and B. V. Shanabrook, *Phys. Rev. Lett.* **78**, 4613 (1997).  
<sup>33</sup>M. Lakrimi, S. Khym, R. J. Nicholas, D. M. Symons, F. M. Peeters, N. J. Mason, and P. J. Walker, *Phys. Rev. Lett.* **79**, 3034 (1997).  
<sup>34</sup>K. Nilsson, A. Zakharova, I. Lapushkin, S. T. Yen, and K. A. Chao, *Phys. Rev. B* **74**, 075308 (2006).  
<sup>35</sup>I. Lapushkin, A. Zakharova, S. T. Yen, and K. A. Chao, *J. Phys.: Condens. Matter* **16**, 4677 (2004).  
<sup>36</sup>M. P. C. M. Krijn, *Semicond. Sci. Technol.* **6**, 27 (1991).  
<sup>37</sup>R. Winkler, M. Merkler, T. Darnhofer, and U. Rössler, *Phys. Rev. B* **53**, 10858 (1996).  
<sup>38</sup>F. Fuchs, J. Schmitz, J. D. Rultson, P. Koidl, R. Heintz, and A. Hoffmann, *Superlattices Microstruct.* **16**, 35 (1994).  
<sup>39</sup>Bradley A. Foreman, *Phys. Rev. Lett.* **81**, 425 (1998).  
<sup>40</sup>H.-R. Trebin, U. Rössler, and R. Ranvaud, *Phys. Rev. B* **20**, 686 (1979).